**Article Title:** Greater mesophyll conductance and leaf photosynthesis in the field through modified cell wall porosity and thickness via AtCGR3 expression in tobacco

**Authors and Affiliations:**

Coralie E. Salesse-Smith[1], Edward B. Lochocki[1], Lynn Doran[1], Benjamin E. Haas[1], Samantha S. Stutz[1], and Stephen P. Long[1,2]

[1]Carl R. Woese Institute for Genomic Biology, University of Illinois at Urbana-Champaign, 1206 W. Gregory Dr., Urbana, IL 61801, USA; [2]Departments of Plant Biology and of Crop Sciences, University of Illinois at Urbana-Champaign, 505 South Goodwin Avenue, Urbana, IL 61801, USA

**Keywords:** Mesophyll conductance, Cell wall thickness, $CO_2$ assimilation, Carbon isotope discrimination, *AtCGR3*, Pectin methyltransferase, water use efficiency, photosynthetic efficiency, Cell wall conductance, Effective porosity

**Word count: 6821**

**Summary**

Mesophyll conductance ($g_m$) describes the ease with which $CO_2$ passes from the sub-stomatal cavities of the leaf to the primary carboxylase of photosynthesis, Rubisco. Increasing $g_m$ is suggested as a means to engineer increases in photosynthesis by increasing [$CO_2$] at Rubisco, inhibiting oxygenation and accelerating carboxylation. Here tobacco was transgenically up-regulated with Arabidopsis Cotton Golgi-related 3 (*CGR3*), a gene controlling methylesterification of pectin, as a strategy to increase $CO_2$ diffusion across the cell wall and thereby increase $g_m$. Across three independent events in tobacco strongly expressing *AtCGR3,* mesophyll cell wall thickness was decreased by 7-13%, wall porosity increased by 75%, and $g_m$ measured by carbon isotope discrimination increased by 28%. Importantly, field-grown plants showed an average 8% increase in leaf photosynthetic $CO_2$ uptake. Upregulating *CGR3* provides a new strategy for increasing $g_m$ in dicotyledonous crops, leading to higher $CO_2$ assimilation and a potential means to sustainable crop yield improvement.

## Introduction

Photosynthesis, the process of converting light energy and atmospheric $CO_2$ into organic compounds, is directly or indirectly the source of all food. Improving photosynthetic efficiency has become a major research objective in order to feed an increasing global population, and to supplement ongoing crop breeding efforts[1,2]. A critical need is to achieve increases without the use of more land or water, given pressures on supply and diminished soil moisture under climate change[3–5]. One strategy with the potential to help meet this challenge is to use genetic engineering to increase photosynthetic efficiency of $C_3$ plants via increased mesophyll conductance[6–8]. However, in order to test this, there is a need to gain a better understanding of mesophyll conductance and how manipulating it may affect photosynthesis and water use efficiency.

Mesophyll conductance ($g_m$) is a measure for the ease with which $CO_2$ from the sub-stomatal cavities may diffuse to the chloroplast stroma, where it is fixed by Rubisco. Increasing $g_m$ can increase photosynthetic capacity of $C_3$ plants, and potentially crop yields, by increasing the concentration of $CO_2$ around Rubisco[7,9]. This would decrease photorespiratory losses and accelerate carboxylation, without any additional cost in transpiration[7,8]. A combination of factors are considered to affect $g_m$. These include gas phase diffusion from the inside of the stomata to exposed mesophyll cell walls and then liquid phase diffusion through the cell wall, plasma membrane, cytosol, chloroplast envelope and chloroplast stroma[10–13].

Mesophyll conductance is influenced by several leaf anatomical properties[10]. Among these are the chloroplast surface area exposed to intercellular airspaces ($S_c$), the mesophyll surface area exposed to intercellular airspaces ($S_m$), and their ratio ($S_c/S_m$), the latter of which has been shown to be positively correlated with $g_m$[14]. Mesophyll cell wall thickness ($T_{cw}$) and porosity, as well as the permeability of the plasma membrane and chloroplast envelope to $CO_2$, are also considered important properties affecting $g_m$[15,16]. Both aquaporins and plastid surface area have been suggested to affect $g_m$[6,17]. However, manipulation studies have produced mixed results[18–21]. Several modelling studies have suggested that the cell wall is one of the most prominent constraints on $g_m$[12,22,23]. Cell wall conductance to $CO_2$ ($g_{cw}$) depends on its thickness, the tortuosity of the path of $CO_2$ through the pores of the cell wall ($\tau$), and the number of those pores (porosity $p$)[10]. Previous studies, including one on natural variation with leaf age in tobacco leaves, have reported that $1/g_m$ has a strong positive correlation with cell wall thickness, inferring that decreasing cell wall thickness is a means to increase $g_m$ [24,25].

Cell wall formation is a complex process involving many genes and their protein products, so there are many potential options for altering cell wall thickness. Previous studies in *A. thaliana* have shown that overexpression of Cotton golgi related 3 (*AtCGR3*) or a functionally redundant gene *AtCGR2* increased the fraction of intercellular airspaces ($f_{ias}$) and plant growth[26,27]. CGR3 is a pectin methyltransferase that catalyzes the methylesterfication of pectin in the cell wall[26]. Essentially, CGR3 adds methyl groups to pectin, serving to increase the extensibility of the cell wall, while affecting porosity [27,28]. Pectin is one of the three main components of dicot primary cell walls, along with cellulose and hemicellulose. Increasing the ratio of pectin to cellulose and hemicellulose or increasing pectin methylation may result in increased cell wall porosity[15,29].

However, neither cell wall thickness, porosity or mesophyll conductance were measured in these prior studies overexpressing CGR3 or CGR2[26,27].

We hypothesized that genetically upregulating CGR3 may improve $CO_2$ diffusion through the cell wall by decreasing its thickness and increasing its porosity, and further hypothesized this in turn would increase $g_m$, $CO_2$ concentration at Rubisco ($C_c$) and, leaf $CO_2$ uptake rate ($A$). This was tested by engineering *AtCGR3* into tobacco and molecular and physiological phenotyping of the resulting events in controlled environments and in the field as a test of concept.

## Results

### Transgenic tobacco expressing AtCGR3

A construct expressing the *Arabidopsis* pectin methyltransferase CGR3 was designed to test the hypothesis that up-regulating CGR3 will decrease the thickness and increase the porosity of the cell wall to improve mesophyll conductance. This construct contains the *Arabidopsis* ubiquitin 10 promoter and 5' leader to drive constitutive expression of *AtCGR3.* As antibodies were not available, a C-terminal FLAG epitope tag was included before the *Arabidopsis* heat shock protein 18 terminator (Figure 1a). The construct was stably transformed into tobacco cv. Samsun, and T2 homozygous plants from three independent single insertion events were characterized in the greenhouse and field. Non-transgenic wildtype (WT) tobacco plants of the genotype transformed and equivalent generation propagated in the same environment were used as controls.

qPCR analysis confirmed that all transgenic lines had high levels of *AtCGR3* RNA expression, while no expression was detected in the WT controls (Figure S1). Immunoblotting was then used to ensure *At*CGR3 protein was accumulating in the transgenic tobacco plants. Strong CGR3 protein expression was observed exclusively in the transgenic plants when probed with anti-FLAG (Figure 1b).

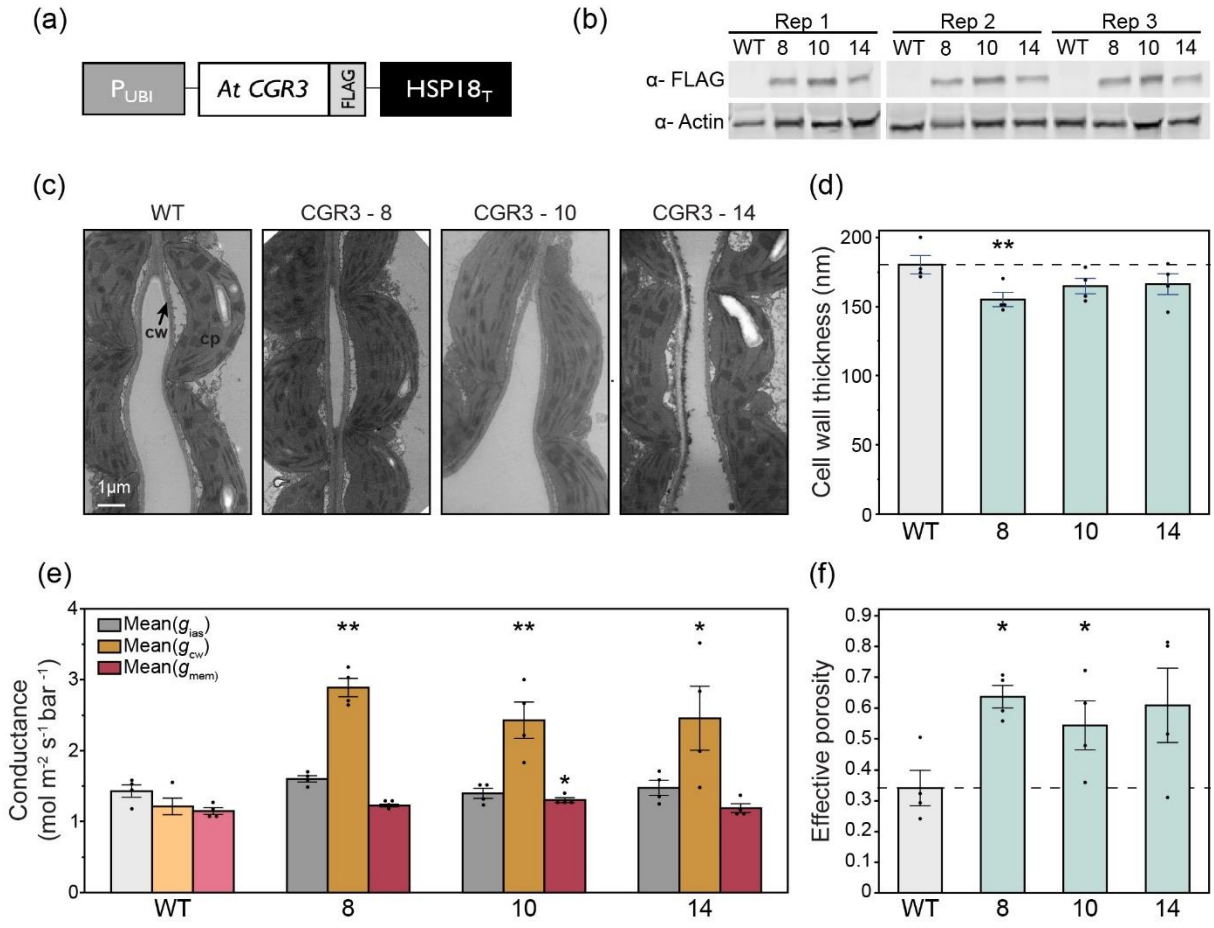


**Figure 1: AtCGR3 protein expression in tobacco and its effect on $CO_2$ conductance across the cell wall.**

**(a)** Transgene designed to constitutively express an Arabidopsis pectin methyltransferase CGR3. The transgene was stably transformed into tobacco cv. Samsun. **(b)** Total soluble protein isolated on a leaf area basis from single copy T2 homozygous plants and analyzed by immunoblot. Three transgenic events (8, 10 and 14) and the wildtype (WT) control were probed with anti-FLAG and anti-Actin antibodies. CGR3 protein is ~28 kDa. Actin was used as a loading control. **(c)** Representative transmission electron micrographs for each event. cw, cell wall; cp, chloroplast. **(d)** Mesophyll wall thickness measured from electron micrographs. **(e)** Estimated $CO_2$ conductances across the intercellular airspace ($g_{ias}$), cell wall ($g_{cw}$), and membranes ($g_{mem}$), expressed on a leaf area basis. **(f)** Estimated effective porosity ($p/\tau$) of the cell wall. Values are shown as the mean $\pm$ SEM (n = 4). Asterisks indicate significant differences between WT and the CGR3 transgenic line (**P < 0.05, *P < 0.1); one-way ANOVA, Dunnett's post hoc test; $g_{cw}$ significance determined with Welch ANOVA, Games-Howell post hoc test.

## AtCGR3 expression increases $CO_2$ conductance across the cell wall

Mesophyll chloroplast ultrastructure observed by transmission electron microscopy showed no differences between genotypes (Figure 1c). Mesophyll cell wall thickness ($T_{cw}$), was decreased 7-13% in the transgenic plants expressing *AtCGR3* (Fig. 1d).

$g_m$ includes $CO_2$ diffusion across multiple sequential barriers, each of which have an associated conductance $g$. The conductances across the intercellular airspace ($g_{ias}$), cell wall ($g_{cw}$) and membranes ($g_{mem}$) are expected to have the largest effects on $g_m$ and can be estimated using measured values of $g_m$, $f_{ias}$, $T_{cw}$, $T_{mes}$, and $S_c$ [30,31]. Using the corresponding measured values presented in Figures 1-3, we calculated that plants expressing AtCGR3 had a significantly increased $g_{cw}$ of 114%, with no significant changes in $g_{ias}$ or $g_{mem}$ (Figure 1e). $g_{cw}$ is directly influenced by cell wall thickness (Figure 1d), porosity and tortuosity[15]. Effective porosity ($p/\tau$) of the cell wall was calculated to have increased by an average 75% compared to the WT control (Figure 1f).

Representative light micrograph images (Figure 2a) show differences in leaf and mesophyll thickness ($T_{mes}$). CGR3 expression resulted in significant increases in the fraction of intercellular airspace ($f_{ias}$) of approximately 12% (Figure 2b), as well as minor increases in $S_c/S_m$ in the three independent transgenic events (Figure 2c). $T_{mes}$ was increased in two of the three independent transgenic events (Figure 2d). Small decreases in leaf mass per unit area (LMA) were observed, however these differences were not significantly different from WT (Table S2).

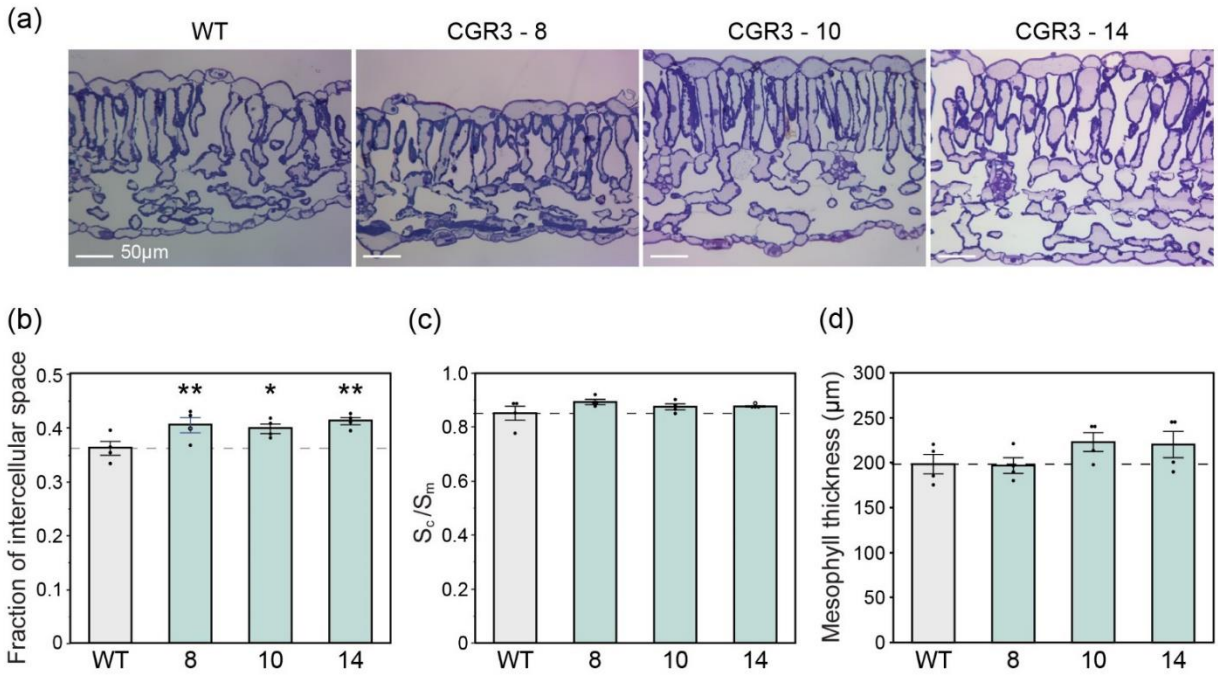


**Figure 2: Light micrographs of transverse leaf sections and measured leaf anatomical traits.**

**(a)** Representative light micrographs. Light micrographs were used to measure **(b)** fraction of intercellular airspace **(c)** ratio of chloroplast surface area exposed to intercellular airspaces ($S_c$) to mesophyll surface area exposed to intercellular airspaces ($S_m$), and **(d)** mesophyll thickness. Values are shown as the mean $\pm$ SEM (n = 4 plants). Asterisks show significant differences between WT and the CGR3 transgenic line (**P < 0.05, *P < 0.1); (b) and (d) one-way ANOVA, Dunnett's post hoc test; (c) Wilcoxon's non-parametric test.

To explore whether CGR3 expression altered cell wall composition, we measured cell wall pectin, hemicellulose and cellulose content. No primary cell wall component showed any significant differences between CGR3 and WT (Table S2). Additionally there was no difference in the ratio of pectin content to the sum of hemicellulose and cellulose content, a value used to indicate cell wall porosity (Table S2)[15].

## Increases in $g_m$ estimated from $\Delta^{13}C$ in transgenic lines grown under controlled growth conditions

Mesophyll conductance was measured to assess whether the anatomical changes described above, including decreased $T_{cw}$ and increased $f_{ias,}$ affect $CO_2$ diffusion. Multiple methods were used to overcome some of the uncertainties associated with estimating $g_m$. First, carbon isotope discrimination ($\Delta^{13}C$) measurements coupled with gas exchange at 2% oxygen were used to estimate $g_m$ in greenhouse grown tobacco. $\Delta^{13}C$ measurements showed that $g_m$ was increased in all three events by an average of 28% relative to WT (Figure 3a). Concomitantly, all three events showed a significantly smaller drawdown of [$CO_2$] between the stomatal cavity and chloroplast stroma ($C_i - C_c$), averaging a 20% less drawdown than WT and therefore a greater [$CO_2$] at Rubisco (Figure 3b). No changes in stomatal conductance ($g_{sw}$) were observed, resulting in significant increases in the ratio of $g_m/g_{sw}$ (Figure 3c). Small increases in $CO_2$ assimilation ($A$) were observed, resulting in indicated increases in intrinsic water use (iWUE; Figure 3d) in all three events, although these were not statistically significant.

Total leaf sugar and starch trended higher in all three transgenic events relative to WT, consistent with increased $CO_2$ assimilation (Figure S2). To check for pleotropic effects from increasing $g_m$, stomatal density and chlorophyll content was measured. All genotypes had similar adaxial and abaxial stomatal densities (Figure S3a-b) and no change in the ratio of abaxial:adaxial stomatal densities was observed (Figure S3c). In addition, leaf chlorophyll content, as measured using a SPAD meter, did not differ between WT and transgenic plants (Table S2).

In addition, $1/g_m$ was significantly lower in all CGR3 events (Table S2) and showed a positive correlation with cell wall thickness ($P$ = 0.0151, $R^2$ = 0.97, Figure 3e), consistent with previous studies[14,24]. In addition, $g_m$ was significantly correlated with effective porosity ($P$ = 0.0615, $R^2$ = 0.88, Figure 3f).

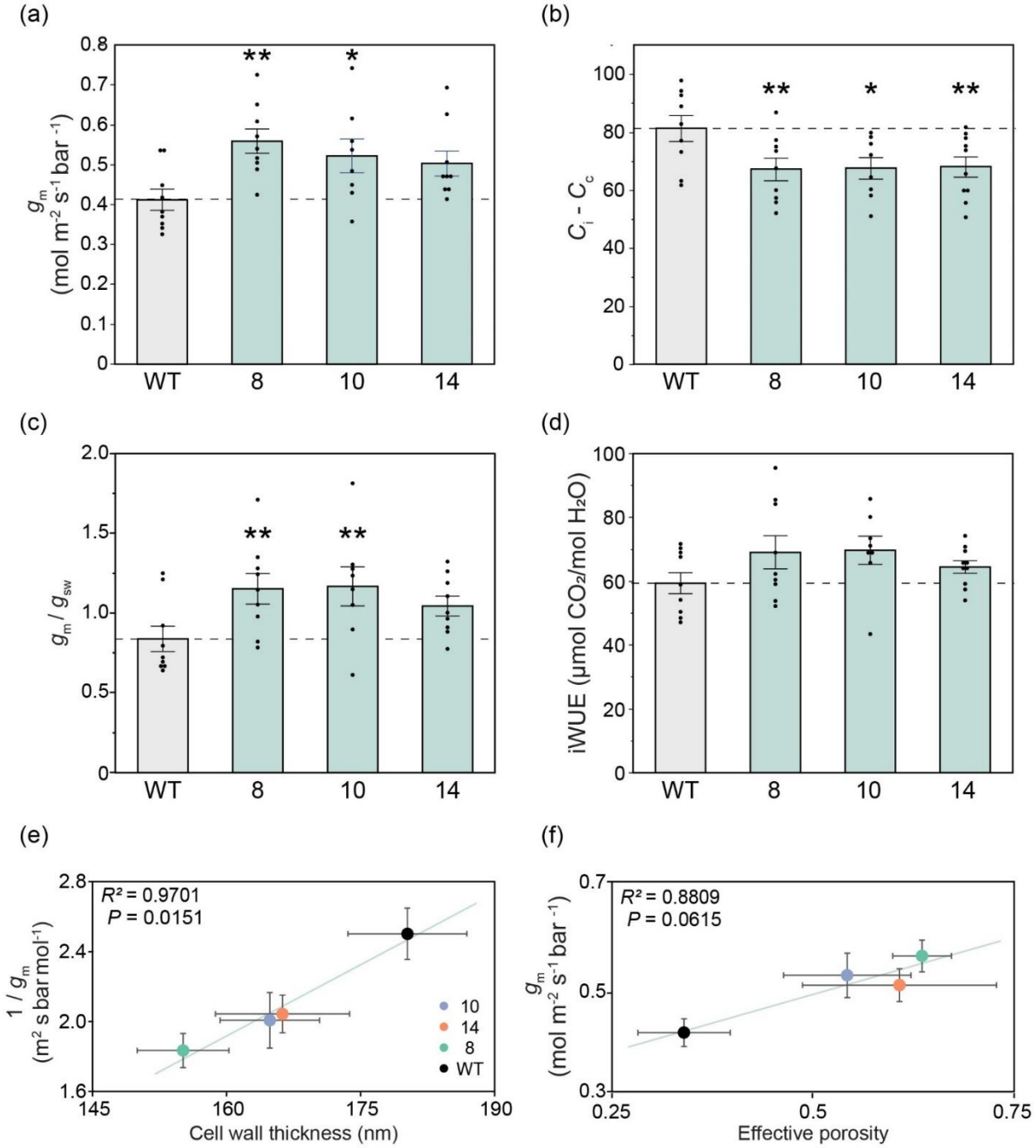


**Figure 3: Mesophyll conductance and associated parameters estimated from carbon isotope discrimination ($\Delta^{13}C$) coupled with gas exchange at 2% oxygen in greenhouse grown tobacco.**

**(a)** Mesophyll conductance ($g_m$) calculated from $\Delta^{13}C$, **(b)** the drawdown of $CO_2$ into the chloroplast ($C_i - C_c$), **(c)** the ratio of mesophyll conductance ($g_m$) to stomatal conductance ($g_{sw}$) and **(d)** intrinsic water use efficiency (iWUE), the ratio of net $CO_2$ assimilation rates ($A$) to stomatal conductance ($g_{sw}$). Measurements were made under the following conditions: light intensity of 1800 µmol m$^{-2}$ s$^{-1}$, leaf temperature of 25 °C, 2% $O_2$, and 400 µmol mol$^{-1}$ $CO_2$.

**(e)** The relationship between $1/g_m$ and mesophyll cell wall thickness and, **(f)** the relationship between $g_m$ and effective porosity. The solid lines represent linear regressions from the data points calculated using Pearson's coefficient of correlation. Values are shown as the mean $\pm$ SEM (n = 4).

## Increased $g_m$ in AtCGR3 events confirmed under field conditions using the Variable *J* method

Subsequently a field experiment was conducted to assess whether differences observed in $g_m$ under greenhouse conditions were reproduced under field conditions. In 2022, a field experiment was carried out with replicated plots of the same three independent transgenic events overexpressing AtCGR3, using a randomized block design (Figure S4a).

Gas exchange measurements were made on the field grown plots to evaluate the physiological effects of decreasing thickness and increasing porosity of the mesophyll cell walls. To test if $g_m$ was altered, gas exchange measurements were made in parallel with chlorophyll fluorescence measurements. We measured $CO_2$ assimilation rates ($A$) as a function of intercellular $CO_2$ concentrations ($C_i$) under saturating light and fit the $A$-$C_i$ curves using the Variable *J* method to derive $g_m$[32,33]. This method models the relationship between $A$, the electron transport rate ($J$), and $C_c$ to estimate $g_m$ over a range of intercellular [$CO_2$] (Figure 4a) and was used because the the tunable laser diode system is not field portable. For each genotype, $g_m$ exhibits a maximum for $C_i$ just below the operating point and decreases for significantly larger or smaller $C_i$, in agreement with previous measurements[34,35]. Measurements made at approximately ambient [$CO_2$] (400 µmol mol$^{-1}$ $CO_2$) showed an average 18% increase in $g_m$ in the CGR3 transgenic plants that was statistically significant, consistent with the prior greenhouse study (Figure 4b). Importantly, and consistent with increased [$CO_2$] at Rubisco, $CO_2$ assimilation rates were significantly increased by an average of 8% in the CGR3 plants relative to the WT controls (Figure 4c). However, $g_{sw}$ was also marginally increased (Figure 4d), resulting in no significant change in intrinsic water use efficiency in the field. No change in the slope of $A$ versus $g_{sw}$ was apparent between WT and the transgenic plants (Figure S6a). Both $g_m$ and $g_{sw}$ had a strong positive correlation with $CO_2$ assimilation (Figure S6).

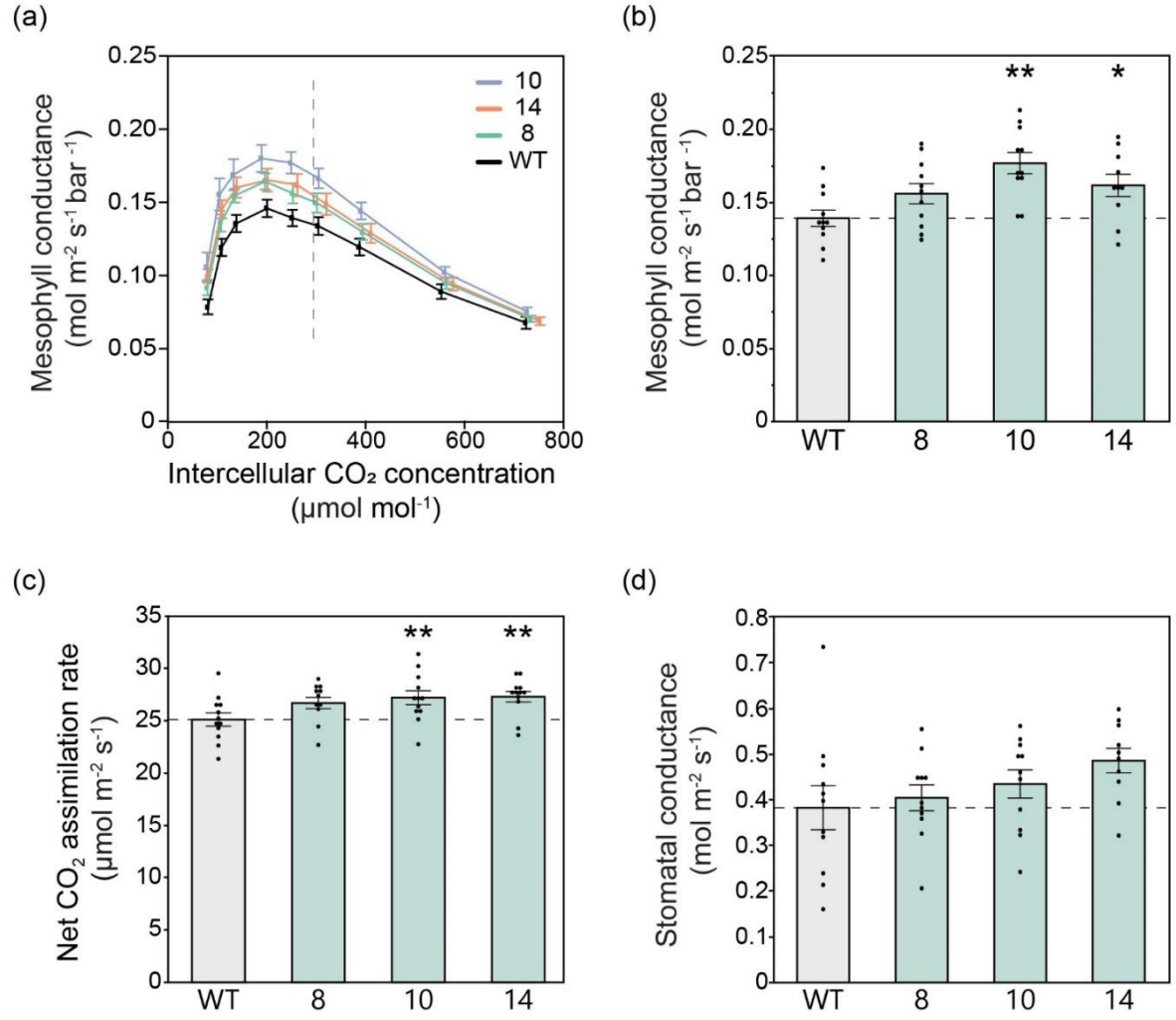


**Figure 4: $CO_2$ assimilation measured with gas exchange in parallel with chlorophyll fluorescence to estimate mesophyll conductance in field grown tobacco plants.**

**(a)** Mesophyll conductance ($g_m$) as a function of intercellular $CO_2$ concentration, estimated using the Variable J method. The vertical dashed line shows the average operating $C_i$ (where ambient $CO_2$ is 420 µmol $mol^{-1}$). **(b)** Mesophyll conductance measured at 400 µmol $mol^{-1}$ $CO_2$ derived from (a). **(c)** Net $CO_2$ assimilation rates and **(d)** stomatal conductance to water ($g_{sw}$), each measured at 400 µmol $mol^{-1}$ $CO_2$. **a-d** measurements made at light intensity of 1800 µmol $m^{-2}$ $s^{-1}$, leaf temperature of 28 °C, and 60% humidity. Values are shown as the mean ± SEM (n =10-11). Asterisks indicate significant difference between WT and the CGR3 transgenic line (**P < 0.05, *P < 0.1); one-way ANOVA, Dunnett's post hoc test.

## $V_{c,max}$ and apparent $V_{c,max}$ estimates from field gas exchange measurements consistent with increased $g_m$ in AtCGR3 transgenic plants

The measured *A*-$C_i$ responses (Figure 5a) were fit to the Farquhar-von-Caemmerer-Berry model [36] to estimate the apparent maximum rate of Rubisco carboxylation ($V_{c,max}$) (Figure 5c). The apparent $V_{c,max}$ value is determined by the initial phase of the relationship of *A* to intercellular

[$CO_2$] ($C_i$), so it is a function of both the actual activity of Rubisco and $g_m$. To test whether the increase in apparent $V_{c,max}$ in the transgenic events was the result of increased $g_m$ or a pleiotropic effect on Rubisco activity, the curves were re-analyzed on a $C_c$ basis, whose values were derived from the $g_m$ obtained at each [$CO_2$] (Figure 4a). The initial phase ($V_{c,max}$) of the transgenic A-$C_c$ curves overlies that of the WT (Figure 5b), showing that the difference was entirely due to increased $g_m$ and not Rubisco activity (Figure 5d).

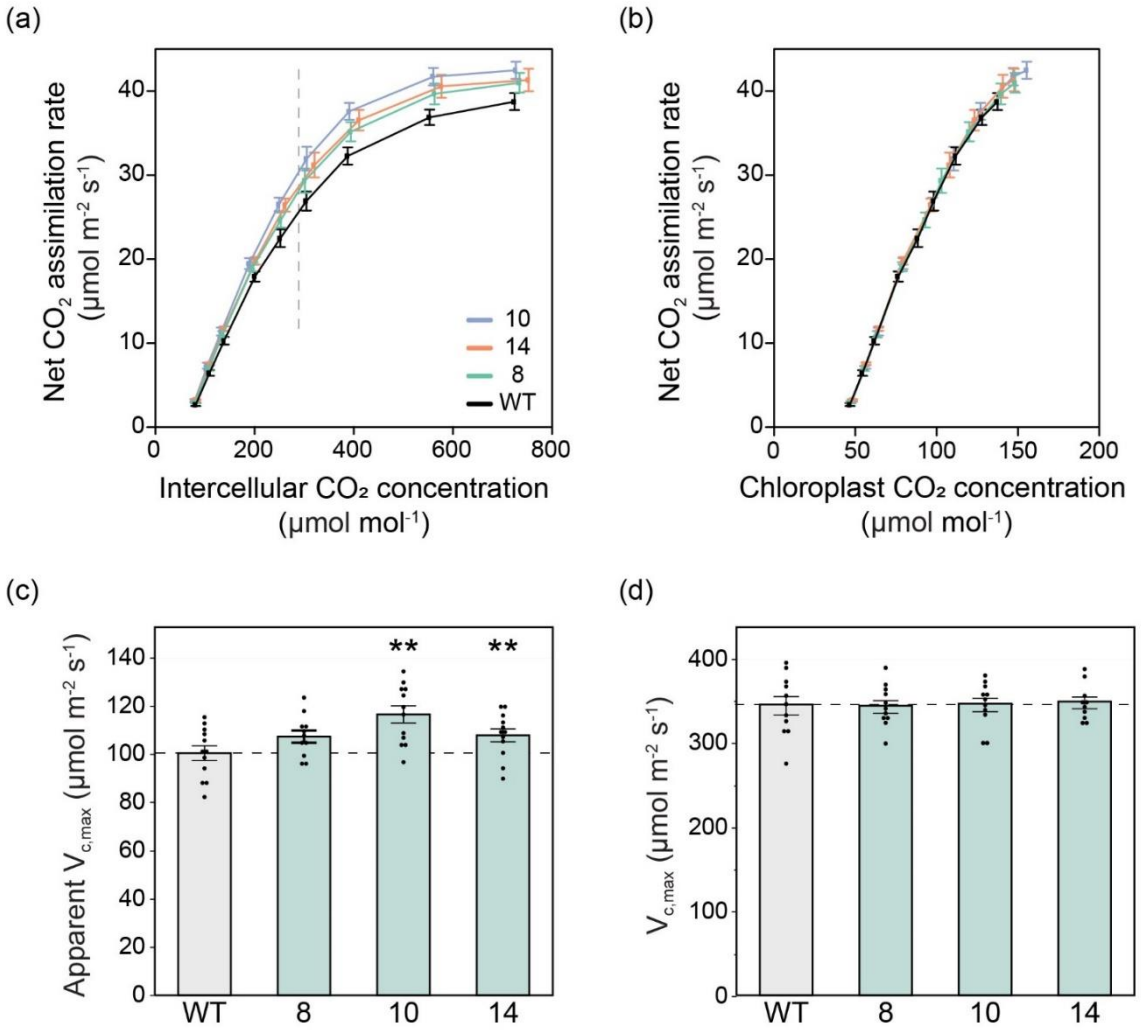


**Fig 5: $CO_2$ response curves and maximum rates of Rubisco carboxylation based on intercellular [$CO_2$] and chloroplast [$CO_2$].**

**(a)** Response of net $CO_2$ assimilation to intercellular [$CO_2$] ($C_i$). Measurements were made under the following conditions: light intensity of 1800 µmol $m^{-2}$ $s^{-1}$, leaf temperature of 28 °C, and 60% humidity. $CO_2$ concentrations varied from 20-1800 µmol $mol^{-1}$ $CO_2$. The vertical dashed line is the average operating $C_i$ (where ambient $CO_2$ is 420 µmol $mol^{-1}$). **(b)** Response of net $CO_2$ assimilation to chloroplast [$CO_2$] ($C_c$). $C_c$ estimated from Variable J fits. **(c)** Apparent maximum Rubisco carboxylation rate ($V_{c,max}$) values at 25 °C estimated from response curves in panel A. $g_m$ equal to infinity. **(d)** Maximum Rubisco carboxylation rate ($V_{c,max}$) values at 25 °C estimated from response curves in panel B. $g_m$ equal to estimated values from Variable J method (Figure 4a). Values are shown as the mean

± SEM (n =10-11). Asterisks indicate significant differences between WT and the CGR3 transgenic line (**P < 0.05); one-way ANOVA, Dunnett's post hoc test.

## Biomass maintained in field-grown plants with decreased cell wall thickness and increased porosity

Cell walls function to protect plants from biotic and abiotic stresses as well as provide structural integrity to the plant, facilitate normal growth and play a crucial role in water relations [37,38]. To assess whether decreased $T_{cw}$ had any negative impacts on plant growth and form in the field, we measured a number of plant growth traits (Figure 6). No significant differences in plant height, leaf area, or total dry biomass were observed between the transgenic lines and control plants (Figure 6 a-c). In addition, there were no changes in leaf number or biomass of leaves, stems or roots when weighed individually (Table S3). We did not observe any differences in structural integrity, lodging, pest or pathogen stress between the AtCGR3 and WT plants; the transgenic lines were essentially indistinguishable from the WT controls (Figure 6d). These results are consistent with growth measurements made in the greenhouse, with the exception that leaf number was significantly increased in the AtCGR3 lines in the greenhouse (Figure S4).

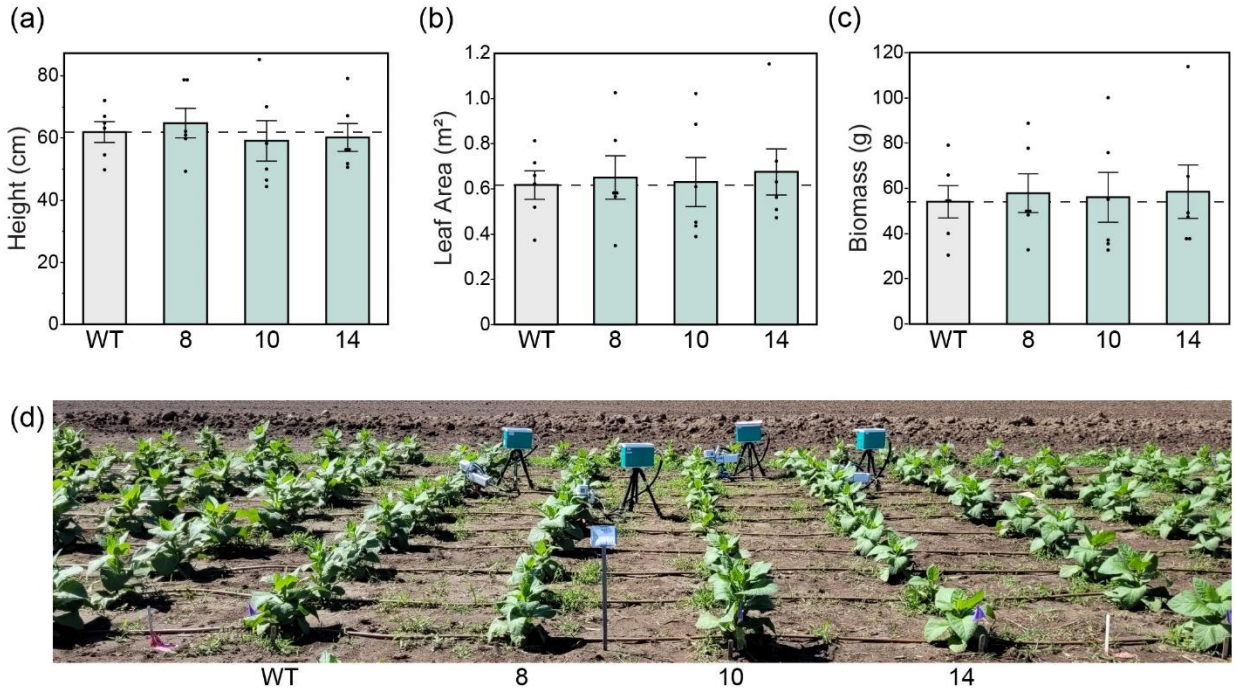


**Figure 6: Plant growth traits in field grown tobacco plants.**

**(a)** Plant height, **(b)** leaf area, and **(c)** biomass (sum of leaf, stem and root dry weights). Values are shown as the mean ± SEM (n = 6 plots). Asterisks indicate significant difference between WT and the CGR3 transgenic line (**P < 0.05, *P < 0.1); (a) and (b) one-way ANOVA, Dunnett's post hoc test; (c) Wilcoxon's non-parametric test. **(d)** Tobacco plants growing in the field in Urbana, Illinois summer 2022.

## Discussion

Increasing the diffusive conductance of $CO_2$ from the atmosphere to Rubisco has been frequently proposed as an important target for improving $CO_2$ assimilation in $C_3$ species[6,7,39,40]. Yet, there have been few successes in engineering a change in $g_m$ into crops. This is at least partly due to an incomplete mechanistic understanding of $g_m$. While aquaporin channels in the plasma membrane and chloroplast surface area were considered prime targets, manipulations have had no or mixed success for $C_3$ species[18,21]. However, observations of variation in both thickness and porosity of the cell wall indicated these as another means to increase mesophyll conductance[15,24]. We identified overexpression of *AtCGR3* as an opportunity to both increase porosity and decrease thickness of the cell wall. Three independent over-expression events in tobacco showed, on average, a 75% increase in porosity and a 10% decrease in thickness of the mesophyll cell walls. This corresponded to a 28% increase in $g_m$ (estimated using two independent methods) and an 8% increase in leaf $CO_2$ assimilation rates, without any pleiotropic effects. This study provides the first report of increased mesophyll conductance via increased porosity and decreased thickness of the cell wall in a dicot species. It also appears one of few demonstrated transgenic increases in mesophyll conductance and leaf photosynthesis of a crop within a replicated field trial[41]. This should serve a proven test-of-concept for further manipulations of the cell wall and application to food crops.

Measured values of $g_m$ are subject to uncertainty because the trait cannot be determined directly and must be estimated using indirect methods. Thus, it is important to check for consistency across different techniques[42] and growth environments. Here, although absolute values are different, similar relative increases in $g_m$ were observed in each of the three transgenic events relative to WT, both when estimated in the field from chlorophyll fluorescence and in the greenhouse from isotopic $^{13}C$ measurements (Figs. 3-4). Previous studies have also shown that isotopic $^{13}C$ measurements result in higher estimates of $g_m$ than the fluorescence Variable *J* method[18,31]. A recent study comparing $g_m$ values measured on the same leaf using both carbon isotope discrimination and chlorophyll fluorescence showed isotopic measurements were consistently higher than fluorescence measurements, with up to a 3-fold difference estimated from measurements made on the same leaf[31]. Reasons for this remain unclear and require further investigation. However, the two sets of values showed a strong linear correlation, indicating that comparisons within each method should be valid. The low $g_m$ values estimated using fluorescence also leads to an overestimation of absolute $V_{c,max}$ values, however this has no effect on relative differences between genotypes. Associated measurements of *A* provide another consistency check. Models predict that increasing $g_m$ on its own should have a modest positive impact on $CO_2$ assimilation rates, as observed here[43]. Further analysis showed that the observed increases in *A* and apparent $V_{c,max}$ were entirely explained by the observed increase in $g_m$ (Figure 5).

Mesophyll conductance is the net effect of several barriers to $CO_2$ diffusion and influenced by several aspects of leaf anatomy. Thus, it is important to identify the main drivers of the

observed increases in $g_m$. To investigate this, measured values of the anatomical traits $f_{ias}$, $T_{mes}$ and $S_c$ were used to calculate $CO_2$ conductance across the intercellular airspace, cell wall and membrane (Figure 1). These results indicated that CGR3 expression increased $g_m$ via increased $CO_2$ conductance across the cell wall, without any change in conductance through the intercellular air space or beyond the wall to Rubisco (Figure 1). Likewise, increased $g_{cw}$ may be due to decreased $T_{cw}$, increased effective porosity, or both. Effective porosity estimated from $g_{cw}$ and $T_{cw}$ shows that both effects are required to explain the increased $g_{cw}$ (Figure 1). It will remain difficult to verify this until methods are established to directly measure effective porosity and each of the conductances within $g_m$, such as a recently published method for quantifying $g_{ias}$[44]. There were other changes in the leaf. LMA was slightly decreased (although this was not significantly different from WT), which would be expected with a slightly smaller investment in cell wall, which can represent 70% of leaf dry mass[45]. Altering leaf anatomy, more specifically mesophyll cell geometry and packing, could influence the distribution of light within the leaf and therefore change leaf absorptance[14]. Although we did not measure absorptance of these plants, no obvious differences were observed in cell geometry, chloroplast thickness or chlorophyll content (Table S2). In addition, our Variable J method makes a best-fit estimate for τ, defined by τ = absorptance x β, where β is the fraction of absorbed light energy directed to photosystem II. The value of β is difficult to experimentally measure and it is often assumed to be 0.5. Variations in τ are expected to be mostly due to variations in absorptance, since it is unlikely that β has been altered in the transgenic plants. No significant differences in τ were observed, indicating that leaf absorptance was likely unchanged across genotypes (Table S3). Cell wall composition analysis showed no differences in total pectin or other cell wall components, consistent with results seen in Arabidopsis, suggesting increases in cell wall effective porosity were due to increased pectin methylation[26]. Glycome profiling of the cell wall could be used to gain more insight on changes in crosslinking within the wall by CGR3 expression and how these alterations affect porosity.

Genetic manipulations can affect multiple traits, making it difficult to identify transgenic manipulations that alter $g_m$ without pleiotropic changes. The few studies successful in increasing $g_m$ and $A$ have either altered additional traits such as true $V_{c,max}$, or are unclear about whether these have been altered, making it difficult to determine if $g_m$ alone can increase photosynthetic rates[41,46–48]. Here we do not observe any changes to the true $V_{c,max}$, i.e. that derived from the response of $A$ to $C_c$ (Figure 5). Decreasing thickness and increasing porosity of the cell wall could be expected to alter mechanical strength of the plant, plant hydraulics, or stomatal function. In the greenhouse and field, there was no observable evidence of any effect on pest damage or plant form. Stomatal density on the adaxial or abaxial leaf surfaces were unchanged, and there was no significant effect on $g_{sw}$ (Table S2; Figure3). Thus, cell wall thickness and porosity has been successfully modified to increase $g_m$ and $A$ without introducing any apparent unintended pleotropic effects.

Despite the significant increase in $A$, no corresponding change in biomass was found in the field. Here, *CGR3* was fused with the *A. thaliana* UBIQUITIN 10, and so the cell wall changes

were likely throughout the plant. It is conceivable that use of the constitutive promoter increased metabolic costs in plant tissue other than leaves, constraining any increase in plant growth. In fact, is has been shown that tissue specific or inducible promoters can be more advantageous than constitutive promoters[49]. Future experiments would ideally use leaf mesophyll specific promoters. Mesophyll specific expression of cell wall properties has been obtained using the Rubisco small subunit 1a (*RBCS1A*) promoter[50].

A major challenge in increasing crop productivity for food security is availability of water[4]. Agriculture accounts for over 70% of water use, and with rising population and climate change, there is little opportunity to gain further water for agricultural use[51]. The air in the sub-stomatal air spaces of leaves is close to water vapor saturation when the outside air has high water vapor pressure[52]. This means that while increased stomatal conductance will result in increased water loss, increased mesophyll conductance should not have a direct effect on water vapor loss from the leaf. Among the several different approaches to increasing photosynthesis to support increased crop productivity, increasing $g_m$ is exceptional in its potential to allow an increase in carbon gain without increased water loss[53]. However, in practice this has not been observed, as $A$ and $g_{sw}$ are strongly correlated, although the mechanistic basis of their interdependence is not well understood[8]. Here, increases in $A$ and $g_m$ in the field-grown plants were balanced by increases in $g_{sw}$, and no changes in iWUE were observed (Figure 4d). It is possible that drought conditions may alter this interdependence, allowing for increased $g_m$, $A$ and iWUE. If true, increased $g_m$ may be most beneficial for sustaining carbon assimilation of plants grown in water limited environments. Our field plants were subjected to temperatures as high at 35 °C in the field, which would have driven large transpiratory fluxes (Figure S5); however, the field plants were irrigated. A recent study by Pathare *et al.* showed engineered increases in $g_m$ resulted in increased biomass of rice plants grown under reduced soil water content but not those subjected to ample water [54]. Taken together these results suggest that follow up studies evaluating the CGR3 overexpression lines under drought stress conditions could be of interest as they may result in improvements in biomass and water use.

Taken together, these results provide a critical proof of concept that increasing $g_m$ by altering the cell wall is a route for enhancing photosynthetic performance of crops. Specifically, the current study shows modification of thickness and porosity as a viable route to improvements in photosynthesis. Gains in water use efficiency could therefore be achieved by combining this increase in $g_m$ with decreased $g_{sw}$, maintaining the same rate of $CO_2$ assimilation while reducing water loss from transpiration. Several approaches have now been identified to allow an engineered or bred decrease in stomatal conductance[55–58]. Stacking increased $g_m$ with other traits such as increased Rubisco activity also has the potential to further increase photosynthetic efficiency. It will be important to consider that certain engineering strategies will only be viable in specific crop species, such as the one here which only applies to $C_3$ dicots. Thus, this work complements previous studies that have modified aquaporins and other aspects of leaf architecture, and extends the engineering “toolbox” available for controlling $g_m$ to further increase photosynthetic efficiency and growth needed to sustainably increase food production.

## Experimental procedures

### Plasmid design and assembly

Vector design and construct assembly followed the genetic syntax of the Phytobrick standard[59] and Loop assembly by Pollak *et al.* (2019)[60]. All required genetic modules were domesticated for BpiI, BsaI and SapI prior to *de-novo* synthesis through TWIST Bioscience. The nucleotide sequence of *A. thaliana* COTTON GOLGI-RELATED 3 (CGR3; AT5G65810.1) was extracted from The Arabidopsis Information Resource (TAIR10)[61] and codon optimized for *N. tabacum* (IDT™ Codon Optimization Tool). Original and codon optimized CGR3 sequences can be found in Data S1. CGR3 was fused with the *A. thaliana* UBIQUITIN 10 (AT4G05320.2) promoter, including the 5'UTR and first intron, a C-terminal 1x FLAG tag and the *A. thaliana* HEAT SHOCK PROTEIN 18.2 3'UTR and terminator (AT5G59720). The CGR3 cassette was combined with a CaMV35S:BAR selection marker and cloned into the pCsB acceptor backbone (Addgene #136068) prior to electroporation into *A. tumefaciens* C58C1. Complete plasmid sequence was verified using next generation sequencing.

### Plant transformation

*N. tabacum* cv. Samsun leaf-disc transformation was performed following Wang (2015)[62]. The following minor modifications were made to the protocol: fully expanded leaf surfaces were submerged in a sterilization solution for 10 minutes. Sterilized leaf discs were rinsed with sterile de-ionized water and cultured in the pre-culture medium. Explants were further incubated at 24°C, with a 16h light period for 48h. *A. tumefaciens* C58C1 containing the target vector was grown overnight to an OD600 of 1.0-1.5 in YEP. Leaf discs were then co-cultivated on fresh pre-culture medium for 48h. After 48h, leaf discs were transferred to a selection medium and incubated under a 16h light period, followed by sub-culturing every 3-4 weeks. Once the shoots reached around 8-10 cm, they were transferred to rooting medium. All media and solution components are described in Methods S1. Established plants were transferred to soil for acclimatization and maturation in the greenhouse after 3-4 weeks.

### Plant growth – greenhouse conditions

T2 homozygous seeds from 3 independent transgenic events and WT *N. tabacum* cv. 'Samsun' seeds from which the transgenics were derived and of the same harvest date were germinated on BM6 growing medium (BM6 All-Purpose, Berger) under greenhouse conditions. Ten days after germination seedlings were transplanted to 9cm x 9cm plastic potting trays. After approximately 2 weeks plantlets were transplanted to 3.8L plastic pots (400C, Hummert International) filled with BM6 growing medium supplemented with 15 $cm^3$ of 15-9-12 (N-P-K) granulated slow-release fertilizer (Osmocote Plus, ICL-Growing Solutions). Plants were grown under natural illumination with ~300 µmol $m^{-2}$ $s^{-1}$ of supplemental light, at 28 °C/12-h days and 22 °C/12 hour nights. Chlorophyll content was measured using a SPAD chlorophyll meter (502, Spectrum Technologies). Leaf mass per area (LMA) was measured from 6 leaf discs each

~1.3cm$^2$ which were dried until constant weight and weights recorded. After approximately 9 weeks of growth tobacco plants were harvested. At harvest leaf number, plant height (equal to stem length) and leaf area (LI-3100C area meter, LI-COR) were measured. Stem and leaves were dried to a constant weight at 60°C and dry weights obtained.

**Transcript and protein expression**

Plants were grown under controlled environment greenhouse conditions described above or field conditions described in a following section. Four leaf discs (each ~1.42 cm$^2$) were sampled from the youngest fully expanded leaf of 9 week old plants between 11:30 h and 13:30 h, flash frozen in liquid nitrogen and stored at -80$^o$C until processed. Tissue was disrupted and homogenized (TissueLyser Universal Laboratory Mixer-Mill disruptor 85210, QIAGEN), at 20 Hz for one and a half minutes twice, submerging cassettes in liquid nitrogen before each run. mRNA was extracted using the NucleoSpin RNA Plant Kit (Macherey-Nagel 740949) modified to increase first RA3 buffer wash to 650 µl and an additional 400 µl RA3 buffer wash. RNA quantity and quality was assessed by NanoDrop™ One/OneC (Thermo Fisher Scientific). cDNA was synthesized using the SuperScript™ III First-Strand Synthesis System (Invitrogen) with random hexamers and 8 µl of RNA.

qPCR was conducted in a 20 µl reaction of SsoAdvanced Universal SYBR Green Supermix (Bio-Rad), dilute cDNA, and 500nmol of each primer and annealing temperature of 59 $^o$C on a CFX Connect Real-Time PCR Detection System (Bio-Rad) at 95 $^o$C for two minutes followed by forty cycles of 95 $^o$C for 15 seconds and 59 $^o$C for 30 seconds. Calibrated Normalized Relative Quantities (CNRQ) were calculated using qBase+ software v.3.2 (CellCarta) based on the expression of two reference genes, Actin and GAPDH. Primers were designed according to MIQE guidelines[63]. Primer linear range and efficiency were determined by qPCR on pooled concentrated cDNA from 4 plots serial diluted by 1:3. Primer efficiencies were between 100-103% with a linear range between 0.15 to 333 ng. See Table S1 for primer sequences used in this study.

Total protein was extracted from 4 leaf discs (each ~1.42 cm$^2$) collected and ground as described above. Tissue was mixed with 1X protein buffer (2.5% BME (v/v), 2 % SDS (w/v), 10 % glycerol (v/v), 0.25 M Tris HCl (pH 6.8)), heated to 95°C for 5 minutes and the quantity expressed per unit leaf area. Proteins were separated on 15-well, 4-20 % Mini-PROTEAN® TGX™ Precast Protein Gel (Bio-rad) and transferred onto polyvinylidene difluoride membranes (Bio-Rad) using the TransBlot®Turbo™ Transfer System (Bio-rad) using the fast TGX protocol. Anti-FLAG (F7425-.2MG, Sigma-Aldrich) and anti-Actin (AS13 2640, Agrisera) primary antibodies were incubated at a 1:5000 dilution overnight at 4 °C in phosphate-buffered saline with 1% non-fat dry milk (w/v) and 0.1% Tween-20. Membranes were incubated with IRDye® 800CW Donkey anti-Rabbit IgG secondary antibody (LI-COR) at a 1:10000 dilution at room temperature for 1-2 hours. Immunoblots were imaged at 800nm using the LI-COR Odyssey CLx Infrared Imaging System (LI-COR).

## Microscopy and anatomical measurements

Leaf tissue was collected from the interveinal region of the youngest fully expanded leaves and fixed in 2% glutaraldehyde (Electron Microscopy Sciences, EMS) and 2.5 % paraformaldehyde (Ted Pella Inc). Fixed tissue was stored at 4°C in the dark until being processed for light and transmission electron microscopy (TEM). Samples were post-fixed in 2% osmium tetroxide (EMS) and potassium ferrocyanide (Mallinkckrodt Baker Inc) and then stained overnight in 7% uranyl acetate at 4°C. A graded series of ethanol, ending in 100% ethanol was used to dehydrate the tissue, followed by 100% acetonitrile. The tissue was then infiltrated with 1:1 acetonitrile to Lx112 epoxy mixture (Ladd, Inc), 1:4 and then pure epoxy before hardening at 80°C overnight. For light microscopy blocks were trimmed and sectioned at 0.35 microns, stained with toluidene-blue and basic fuchsin, and viewed with a stereo microscope (BH2, Olympus) coupled with an ocular digital camera (AMT). For electron microscopy blocks were sectioned at 60-90nm for electron microscopy and viewed at 75KV where plate film was scanned in at 3200 dpi (H600, Hitachi).

Light micrographs were used to measure the length of mesophyll cells exposed to intercellular airspace ($L_{mes}$), the length of chloroplast exposed to intercellular airspace ($L_c$) and the width of each section measured ($W$). Mesophyll surface area exposed to intercellular airspace ($S_{mes}$) and chloroplast surface area exposed to intercellular ($S_c$) were calculated using Equations 4 and 6 from Evans *et al.* (1994)[64].

At least three non-overlapping fields of view were randomly selected to provide technical replicates, which were averaged to provide a single value for each of the four biological replicates for each genotype. Transmission electron micrographs were used to measure mesophyll cell wall thickness. 10 non-overlapping fields of view were measured from each of the four biological replicates per genotype. For each image (technical replicate) the area of the cell wall divided by the length was used to calculate cell wall thickness. A total cell wall length of approximately 6500 nm was measured per genotype. This accounts for small variations in thickness along the cell wall. Technical replicates were averaged to provide a single value for each biological replicate (4 per genotype). All measurements were made using the freehand area and line selection tools from ImageJ (National Institutes of Health).

## Leaf and Cell wall composition analysis

Fully expanded leaves with midrib excised were flash frozen in aluminum foil packets in liquid nitrogen before storage at -80°C. Three to six grams of tissue were lyophilized to a steady state weight. Lyophilized tissue was ground for 15 minutes at 1200 rpm on a Genogrinder 2010 (SPEX) using two 4 mm stainless steel grinding beads. Total sugars were extracted from 100-200 mg of ground, dried tissue by incubation in 80% ethanol at 80°C for 20 minutes with decantation six times [65]. Ethanol extracts were treated with activated charcoal to remove compounds such as lactic acid, sugar alcohols, and alcohol-soluble pigments which can interfere in the reaction and lead to overestimations of sugar content. Total sugar as glucose was measured using the sulfuric-phenol microplate assay as described in Kondo *et al.* (2021)[66]. The

protocol was modified to change the heat treatment to 90 °C in a water bath for 5 minutes. Sugar extract absorbance at 490 nm was measured in triplicate on a Synergy HI Microplate spectrophotometer (Biotek) against a 5-25 ug glucose standard curve.

After ethanol extraction the remaining pellet was washed with 1:1 chloroform:methanol (v/v), followed by acetone, and dried overnight at 35°C. The pellet was subjected to three rounds of digestion by 500 µL of 120 U/mL α-amylase Bacillus licheniformis (Neogen) in 10 mM, pH 6.5 MOPS buffer at 75 °C for 30 minutes [65]. The enzyme was deactivated by heating at 99 °C for 10 minutes. After centrifugation at 13,000 g for 10 minutes, 800 µl of supernatant was quantitatively transferred and subjected to two rounds of digestion by 500 µL of 30 U/mL amyloglucosidase Aspergillus niger (Neogen) in 100mM, pH 4.5 acetate buffer at 50 °C for 30 minutes [65]. Total starch as glucose was measured by D-Glucose GOP-POD microplate assay (nzytech). The pellet from the α-amylase MOPS digestion was decanted, washed with water twice, and acetone once. The acetone was removed using a Speed Vac Concentrator (Thermo Fisher Scientific) to steady state weight resulting in the cell wall alcohol insoluble residue (AIR).

In triplicate, 2-3 mg of AIR was digested in 375 µl 2 M trifluoroacetic acid (TFA) at 121°C for 90 minutes[67]. Supernatant was removed and analyzed for TFA soluble hemicellulose by the sulfuric-phenol microplate assay described previously and for pectin as D-Galacturonic acid per Bethke and Glazebrook (2019)[68] with minor modifications. The addition of 2 mg/mL prepared m-hydroxydiphenyl reagent was reduced to 10 µl per well and measured absorbance at 525 nm in triplicate on a Synergy HI Microplate spectrophotometer (Biotek) against a 6.25 to 200 nmol D-(+)-galacturonic acid monohydrate (AAJ6628214, Thermo Fisher Scientific) standard curve.

Cellulose and non-soluble hemicellulose (primarily glycan) was digested with sulfuric acid as described in Foster, Martin, and Pauly (2010)[67] and quantified as glucose by the sulfuric-phenol microplate assay described previously against a 2-12 µg glucose standard curve. Detailed protocol available at protocols.io. https://dx.doi.org/10.17504/protocols.io.3byl4q6jzvo5/v1.

**Stomatal density**

Adaxial and abaxial stomatal impressions of approximately 2 $cm^2$ were made on the youngest fully expanded leaf of greenhouse grown plants as described previously[69]. Six plants per genotype were sampled. Four images were obtained per impression using the Axio Imager A1 microscope (Zeiss) equipped with the Zeiss AxioCam HrC digital camera, AxioVision software version 4.9.1.0 (Zeiss) and a 20x/0,5 objective (EC Plan-Neofluar420350-9900). All whole stomata and partial stomata on the left and top borders of the image were counted using Cell Counter Plugin (https://imagej.net/ij/plugins/cell-counter.html) in ImageJ [70] and used to calculate stomatal density.

**Estimating mesophyll conductance using carbon isotope discrimination coupled with leaf gas exchange**

The LI-COR 6800 gas exchange system (LI-COR Environmental) was coupled to a tunable-diode laser absorption spectroscope (TDLAS model TGA 200A; Campbell Scientific) to measure online carbon isotope discrimination [71,72]. The TDL was connected to the LI-6800 reference and sample air streams using the ports on the back of the sensor head. $N_2$ and $O_2$ were mixed using mass flow controllers (OMEGA Engineering Inc.) and spilt into multiple lines to use as $CO_2$ free air. One line was used to zero the TDL throughout the measurements. Two lines supplied the inlets of two gas exchange systems to make measurements at 2% $O_2$. The final line was diluted with a 10% $CO_2$ gas cylinder to produce three different $CO_2$ concentrations (60, 300 and ~1000 ppm $CO_2$) of the same isotopic signature and used to calibrate the $^{13}CO_2$ signal.

The measurements cycled through nine gas streams in the following sequence: calibration zero, calibration points 60, 300 and 1000 ppm $CO_2$, NOAA calibration of $\delta^{13}C$ composition (NOAA Global Monitoring Laboratory), LI-COR 6800 #1 reference and leaf chamber air streams, and LI-COR 6800 #2 reference and leaf chamber air streams. Each step had a duration of 20 s and measurements were averaged over the last 10 s to produce a single data point.

Gas exchange measurements were made under the following conditions: light intensity of 1800 µmol $m^{-2}$ $s^{-1}$, leaf temperature of 25°C, leaf vapor pressure deficit of 1.3 kPa, 2% $O_2$, and 400 µmol $mol^{-1}$ $CO_2$. Two percent oxygen was used to minimize photorespiration. Once steady-state $CO_2$ assimilation and stomatal conductance were reached the gas-exchange system was set to auto-log at 180 s intervals over the course of 30 min. After the program was completed, the light was turned off and dark respiration rate was measured on plants after >30 minutes in the dark.

The combined gas exchange and TDLAS data were processed and analyzed using PhotoGEA, an R package for photosynthetic gas exchange analysis [73]. This process generally followed the steps described in the "Analyzing Mesophyll Conductance Data" article included with PhotoGEA, which is also available online at the PhotoGEA documentation website: https://eloch216.github.io/PhotoGEA/.

Within each TDL cycle, correction factors derived from the five calibration tanks were used to obtain calibrated dry-air [$^{12}CO_2$] and [$^{13}CO_2$] in the air streams entering and exiting each LI-COR leaf chamber. The isotopic composition ($\delta^{13}C$) of each air stream was calculated using Equation 4 from Ubierna *et al*. (2018)[74]. Timestamps and TDL valve numbers were then used to pair each TDL measurement with its corresponding gas exchange log entry, enabling the calculation of the observed photosynthetic $^{13}CO_2$ discrimination ($\Delta^{13}C$) and the ternary gas correction factor ($t$) using Equations 5 and 9 from Ubierna *et al*. (2018) [74]. The $CO_2$ compensation point in the absence of day respiration ($\Gamma^*$) was calculated from [$O_2$] and leaf-temperature-dependent $O_2$ and $CO_2$ solubilities assuming a Rubisco specificity of 97.3 M $M^{-1}$ [75]. Finally, mesophyll conductance to $CO_2$ diffusion ($g_{mc}$) was calculated using Equations 13 and 22 from Busch *et al*. (2020) [35], which assume that mitochondrial respiration is isotopically disconnected from the Calvin-Benson-Bassham cycle. The effective isotopic fractionation due to day respiration ($e^*$) was calculated using Equation 19 from Busch *et al*. (2020) [35] rather than Equation 20, because values of $\Delta_{obs}^{growth}$ were not available; however, this should have minimal impact due to the low [$O_2$] used for these measurements.

## Plant growth – field conditions

Seeds from homozygous T2 single insertion events (CGR3-8, CGR3-10 and CGR3-14) and WT seed from the same harvest date were sown in the greenhouse on May 16th 2022 (DOY 136). After 10 days seedlings were transplanted to floating trays as described in Kromdijk *et al.* (2016)[76]. Plantlets were transplanted to the University of Illinois Energy farm field site (40.11°N, 88.21°W, Urbana, IL, USA) on June 10th 2022 (DOY 161). The field was prepared one week prior to transplant as described previously[76].

The field experiment used a randomized block design with six blocks. Each block consisted of 4 rows of 10 plants per genotype in a north-south (N-S) orientation, with plants spaced 61 cm apart (Figure S5a). Each block contained one WT row. In addition, one border row of WT plants surrounded the perimeter of the 6 experimental blocks. Plants were irrigated as needed using parallel drip irrigation lines (DL077, The Drip Store). Weather data were measured with a digital sensor mounted 10 m above ground level at the same field site (ClimaVUE50, Campbell Scientific, Figure S5b-c).

Plants were harvested July 21st 2022 (DOY 202). At harvest leaf number, plant height (equal to stem length) and leaf area (LI-3100C area meter, LI-COR) were measured. Harvested material was partitioned into leaf, stem and roots for 5 randomly selected plants per row. These were dried to a constant weight at 60°C in custom built dying ovens and dry weights obtained.

## Leaf gas exchange in the field

Photosynthetic gas exchange measurements were performed on the youngest fully expanded leaves on July 9th - 10th 2022 (DOY 190-191). $CO_2$ response curves (A-$C_i$) were measured using a LI6800 infrared gas exchange system with integrated leaf chamber fluorometer (LI-COR). Leaves were clamped into a 6 $cm^2$ gas exchange cuvette and acclimated to the following conditions: light intensity of 1800 µmol $m^{-2}$ $s^{-1}$, leaf temperature of 28 °C, $CO_2$ reference concentration of 400 µmol $mol^{-1}$ and 60% humidity. $CO_2$ responses were initiated when rates of $CO_2$ assimilation and stomatal conductance stabilized to a steady state (~20 min). Response curve were measured with the following sequence of reference [$CO_2$]: 400, 300, 200, 150, 75, 50, 20, 400, 400, 500, 600, 800, 1000, 1200, 1500, and 1800 µmol $m^{-2}$ $s^{-1}$. Measurements were logged 3 to 5 minutes after each new [$CO_2$] step. Fluorescence measurements were made at each step using the multi-phase flash fluorescence protocol with a saturating flash of 10,000 µmol $m^{-2}$ $s^{-1}$.

Apparent maximum Rubisco carboxylation rates ($V_{c,max}$) at 25 °C were estimated using the *fit_c3_aci* function from the PhotoGEA R package [73], which fits measured $CO_2$ response curves with the Farquhar-von-Caemmerer-Berry (FvCB) model, including limitations from triose phosphate utilization (TPU) [36]. Temperature scaling of key parameters ($K_C$, $K_O$, Γ*, $V_{c,max}$, $J$, and $R_d$) was modeled using Arrhenius factors [77] and mesophyll conductance was set to infinity

(equivalent to setting $C_c = C_i$). During the fits, an optimization algorithm is used to choose values of the four unknown FvCB model parameters ($V_{c,max}$, $J$, and $R_d$ at 25 °C and the maximum rate of TPU, $T_p$) that produce the best agreement between the modeled and measured $CO_2$ assimilation rates.

**Estimating mesophyll conductance using Variable *J***

$C_c$, $g_{mc}$, and the true $V_{c,max}$ were estimated from gas exchange measurements made in parallel with chlorophyll fluorescence measurements using the "Variable *J*" fitting method as implemented in the *fit_c3_variable_j* function from the PhotoGEA R package [73]. In this method, net $CO_2$ assimilation ($A_n$) is modeled by (1) calculating $g_{mc}$ and $C_c$ from the incident photosynthetically active photon flux density ($Q_{in}$), the measured operating efficiency of photosystem II ($\phi_{PSII}$), and the measured $A_n$, and then (2) using the calculated $C_c$ as an input to the FvCB model [32,33]. There are five unknowns in the equations used to model $A_n$: $\tau$ (a proportionality factor that relates $Q_{in}$ and $\phi_{PSII}$ to the fluorescence-based estimate of the RuBP regeneration rate) and the four FvCB model parameters ($V_{c,max}$, $J$, and $R_d$ at 25 °C and $T_p$). During the fits, an optimization algorithm is used to choose values of these unknowns that produce the best agreement between the measured and modeled $A_n$. Once these parameter values have been found, values of $C_c$ and $g_{mc}$ are also immediately known.

**Estimation of effective porosity**

The cell wall effective porosity ($p$ / $\tau$) can be determined from the cell wall conductance to $CO_2$ diffusion ($g_{cw}$) provided the cell wall thickness $T_{cw}$ is known [78]. In turn, $g_{cw}$ can be estimated from $g_{mc}$ by accounting for the effect of other known barriers to $CO_2$ diffusion (specifically, the intercellular airspace, the plasma membrane, and the chloroplast envelope) [31,78]. Here we use this approach to calculate $p$ / $\tau$ from measured values of $g_{mc}$, $f_{ias}$, $T_{cw}$, $T_{mes}$, and $S_c$. Overall, our method is similar to the one used in Ellsworth *et al*. (2018) [78], but differs by including the conductance across the intercellular airspace and a membrane conductance enhancement factor as in Xiong (2023)[31]. For details of the calculations, see Methods S2.

**Statistical analysis**

Normality of the data was tested with Shapiro-Wilk's test, and homoscedasticity with Brown-Forsythe's test. If criteria for normal distributions and equal variance was met one-way ANOVA followed by Dunnett's *post hoc* test for transgenic mean comparison against the WT control was performed. Data were considered significant at $P < 0.05$ and marginally significant at $P < 0.1$. If criteria for normality was violated, Wilcoxon's non-parametric test was applied. If criteria for equal variance was violated Welch's ANOVA followed by Games-Howell post hoc test was applied. Analysis of field growth traits (Figure 6) was performed using a randomized block design with 6 blocks. Tests used are indicated in the figure or table legend. Correlations

between $1/g_m$ and $T_{cw}$, and $g_m$ and effective porosity were evaluated using Pearson's correlation coefficient. Jmp pro version 17.0.0 software was used for all statistical analyses.

## Author Contributions

CES and SPL designed the experiments. BEH assembled the construct and supervised generation of the transgenic tobacco lines. SSS set up the TDL and maintained the carbon isotope discrimination equipment. LD measured gene expression, cell wall composition and stomatal density. EBL calculated effective porosity, $g_{ias}$, $g_{cw}$, and $g_{mem}$, and developed the PhotoGEA data-processing R package used to analyze all gas exchange and carbon isotope discrimination data. CES participated in all experiments and analyzed the data. CES and SPL wrote the manuscript with contributions from all authors.


## Acknowledgements

We thank Mike Root for the transformation and tissue culture of tobacco. We thank David Drag, Ben Harbaugh, Ben Thompson, Ron Edquilang and Andrew Wszalek for help with the maintenance of greenhouse plants, field experiment and field harvest. We also thank Noga Adar, Maddie Burke and Amanda Eggers for technical lab support. The microscopy work was carried out in part in the Materials Research Laboratory Central Research Facilities, University of Illinois. This work supported by the Bill & Melinda Gates Foundation, Foundation for Food and Agriculture Research and the UK Foreign, Commonwealth & Development Office under grant no. OPP11722157, and from Bill & Melinda Gates Agricultural Innovations grant investment ID 57248.


## Conflict of Interest

The authors declare no conflicts of interest.

## Short legends for Supporting Information

Figure S1| Gene expression in field grown CGR3 and WT lines.
Figure S2| Sugar and starch content of greenhouse grown tobacco plants.
Figure S3| Stomatal density of greenhouse grown tobacco plants.
Figure S4| Plant growth traits in greenhouse grown tobacco plants.
Figure S5| Tobacco field experimental design and weather conditions.
Figure S6| Correlation of $CO_2$ assimilation to stomatal and mesophyll conductance.
Table S1: qPCR primer information
Table S2: Summary of leaf gas exchange combined with carbon isotope discrimination, cell wall composition, leaf mass per area (LMA) and chlorophyll content (SPAD value) of greenhouse grown plants.

Table S3: Summary of harvest measurements from field-grown plants.
Methods S1. Plant transformation culture media and solutions components.
Methods S2. Details for estimation of effective porosity
Data S1. Codon optimized sequence of AtCGR3

## References


1. Ray, D. K., Mueller, N. D., West, P. C. & Foley, J. A. Yield Trends Are Insufficient to Double Global Crop Production by 2050. *PLOS ONE* **8**, e66428 (2013).
2. Bailey-Serres, J., Parker, J. E., Ainsworth, E. A., Oldroyd, G. E. D. & Schroeder, J. I. Genetic strategies for improving crop yields. *Nature* **575**, 109–118 (2019).
3. Dai, A. Increasing drought under global warming in observations and models. *Nat. Clim. Change* **3**, 52–58 (2013).
4. Ort, D. R. & Long, S. P. Limits on Yields in the Corn Belt. *Science* **344**, 484–485 (2014).
5. Hunter, M. C., Smith, R. G., Schipanski, M. E., Atwood, L. W. & Mortensen, D. A. Agriculture in 2050: Recalibrating Targets for Sustainable Intensification. *BioScience* **67**, 386–391 (2017).
6. Lundgren, M. R. & Fleming, A. J. Cellular perspectives for improving mesophyll conductance. *Plant J.* **101**, 845–857 (2020).
7. Flexas, J. *et al.* Diffusional conductances to CO2 as a target for increasing photosynthesis and photosynthetic water-use efficiency. *Photosynth. Res.* **117**, 45–59 (2013).
8. Leakey, A. D. B. *et al.* Water Use Efficiency as a Constraint and Target for Improving the Resilience and Productivity of C3 and C4 Crops. *Annu. Rev. Plant Biol.* **70**, 781–808 (2019).
9. Perez-Martin, A. *et al.* Interactive effects of soil water deficit and air vapour pressure deficit on mesophyll conductance to CO2 in Vitis vinifera and Olea europaea. *J. Exp. Bot.* **60**, 2391–2405 (2009).

10. Evans, J. R. Mesophyll conductance: walls, membranes and spatial complexity. *New Phytol.* **229**, 1864–1876 (2021).
11. Cousins, A. B., Mullendore, D. L. & Sonawane, B. V. Recent developments in mesophyll conductance in C3, C4, and crassulacean acid metabolism plants. *Plant J.* **101**, 816–830 (2020).
12. Xiao, Y. & Zhu, X.-G. Components of mesophyll resistance and their environmental responses: A theoretical modelling analysis. *Plant Cell Environ.* **40**, 2729–2742 (2017).
13. Salesse-Smith, C. E., Driever, S. M. & Clarke, V. C. Modifying mesophyll conductance to optimise photosynthesis in crops. in *Burleigh Dodds Series in Agricultural Science* (eds. Western Sydney University, Australia & Sharwood, R.) (Burleigh Dodds Science Publishing, 2023). doi:10.19103/AS.2022.0119.10.
14. Ren, T., Weraduwage, S. M. & Sharkey, T. D. Prospects for enhancing leaf photosynthetic capacity by manipulating mesophyll cell morphology. *J. Exp. Bot.* **70**, 1153–1165 (2019).
15. Flexas, J. *et al.* Cell wall thickness and composition are involved in photosynthetic limitation. *J. Exp. Bot.* **72**, 3971–3986 (2021).
16. Carriquí, M. *et al.* Cell wall composition strongly influences mesophyll conductance in gymnosperms. *Plant J.* **103**, 1372–1385 (2020).
17. Momayyezi, M., McKown, A. D., Bell, S. C. S. & Guy, R. D. Emerging roles for carbonic anhydrase in mesophyll conductance and photosynthesis. *Plant J.* **101**, 831–844 (2020).
18. Kromdijk, J., Głowacka, K. & Long, S. P. Photosynthetic efficiency and mesophyll conductance are unaffected in Arabidopsis thaliana aquaporin knock-out lines. *J. Exp. Bot.* **71**, 318–329 (2020).
19. Uehlein, N. *et al.* Function of Nicotiana tabacum Aquaporins as Chloroplast Gas Pores Challenges the Concept of Membrane CO2 Permeability. *Plant Cell* **20**, 648–657 (2008).
20. Heckwolf, M., Pater, D., Hanson, D. T. & Kaldenhoff, R. The Arabidopsis thaliana aquaporin AtPIP1;2 is a physiologically relevant CO2 transport facilitator. *Plant J.* **67**, 795–804 (2011).

21. Głowacka, K. *et al.* Is chloroplast size optimal for photosynthetic efficiency? *New Phytol.* **239**, 2197–2211 (2023).
22. Yin, X. & Struik, P. C. Can increased leaf photosynthesis be converted into higher crop mass production? A simulation study for rice using the crop model GECROS. *J. Exp. Bot.* **68**, 2345–2360 (2017).
23. Gago, J. *et al.* Mesophyll conductance: the leaf corridors for photosynthesis. *Biochem. Soc. Trans.* **48**, 429–439 (2020).
24. Clarke, V. C., Danila, F. R. & von Caemmerer, S. CO2 diffusion in tobacco: a link between mesophyll conductance and leaf anatomy. *Interface Focus* **11**, 20200040 (2021).
25. Onoda, Y. *et al.* Physiological and structural tradeoffs underlying the leaf economics spectrum. *New Phytol.* **214**, 1447–1463 (2017).
26. Kim, S.-J., Held, M. A., Zemelis, S., Wilkerson, C. & Brandizzi, F. CGR2 and CGR3 have critical overlapping roles in pectin methylesterification and plant growth in Arabidopsis thaliana. *Plant J.* **82**, 208–220 (2015).
27. M. Weraduwage, S. *et al.* Pectin Methylesterification Impacts the Relationship between Photosynthesis and Plant Growth. *Plant Physiol.* **171**, 833–848 (2016).
28. Wu, H.-C., Bulgakov, V. P. & Jinn, T.-L. Pectin Methylesterases: Cell Wall Remodeling Proteins Are Required for Plant Response to Heat Stress. *Front. Plant Sci.* **9**, 1612 (2018).
29. Roig-Oliver, M. *et al.* Reduced photosynthesis in Arabidopsis thaliana atpme17.2 and atpae11.1 mutants is associated to altered cell wall composition. *Physiol. Plant.* **172**, 1439–1451 (2021).
30. Evans, J. R. & von Caemmerer, S. Temperature response of carbon isotope discrimination and mesophyll conductance in tobacco. *Plant Cell Environ.* **36**, 745–756 (2013).
31. Xiong, D. Leaf anatomy does not explain the large variability of mesophyll conductance across C3 crop species. *Plant J.* **113**, 1035–1048 (2023).

32. Moualeu-Ngangue, D. P., Chen, T.-W. & Stützel, H. A new method to estimate photosynthetic parameters through net assimilation rate−intercellular space CO2 concentration (A−Ci) curve and chlorophyll fluorescence measurements. *New Phytol.* **213**, 1543–1554 (2017).
33. Harley, P. C., Loreto, F., Di Marco, G. & Sharkey, T. D. Theoretical Considerations when Estimating the Mesophyll Conductance to CO2 Flux by Analysis of the Response of Photosynthesis to CO2 1. *Plant Physiol.* **98**, 1429–1436 (1992).
34. Flexas, J. *et al.* Rapid variations of mesophyll conductance in response to changes in CO2 concentration around leaves. *Plant Cell Environ.* **30**, 1284–1298 (2007).
35. Busch, F. A., Holloway-Phillips, M., Stuart-Williams, H. & Farquhar, G. D. Revisiting carbon isotope discrimination in C3 plants shows respiration rules when photosynthesis is low. *Nat. Plants* **6**, 245–258 (2020).
36. von Caemmerer, S. *Biochemical Models of Leaf Photosynthesis*. (Csiro Publishing, 2000).
37. Hückelhoven, R. Cell Wall–Associated Mechanisms of Disease Resistance and Susceptibility. *Annu. Rev. Phytopathol.* **45**, 101–127 (2007).
38. Taiz, L. Plant Cell Expansion: Regulation of Cell Wall Mechanical Properties. *Annu. Rev. Plant Physiol.* **35**, 585–657 (1984).
39. Flexas, J. *et al.* Mesophyll conductance to CO2 and Rubisco as targets for improving intrinsic water use efficiency in C3 plants. *Plant Cell Environ.* **39**, 965–982 (2016).
40. Zhu, X.-G., Long, S. P. & Ort, D. R. Improving photosynthetic efficiency for greater yield. *Annu. Rev. Plant Biol.* **61**, 235–261 (2010).
41. Xu, F. *et al.* Overexpression of rice aquaporin OsPIP1;2 improves yield by enhancing mesophyll CO2 conductance and phloem sucrose transport. *J. Exp. Bot.* **70**, 671–681 (2019).
42. Pons, T. L. *et al.* Estimating mesophyll conductance to CO2: methodology, potential errors, and recommendations. *J. Exp. Bot.* **60**, 2217–2234 (2009).

43. Clarke, V. C. *et al.* Mesophyll conductance is unaffected by expression of Arabidopsis PIP1 aquaporins in the plasmalemma of Nicotiana. *J. Exp. Bot.* **73**, 3625–3636 (2022).
44. Márquez, D. A., Stuart-Williams, H., Cernusak, L. A. & Farquhar, G. D. Assessing the CO2 concentration at the surface of photosynthetic mesophyll cells. *New Phytol.* **238**, 1446–1460 (2023).
45. Ye, M. *et al.* High leaf mass per area Oryza genotypes invest more leaf mass to cell wall and show a low mesophyll conductance. *AoB PLANTS* **12**, plaa028 (2020).
46. Gong, H. Y. *et al.* Transgenic Rice Expressing Ictb and FBP/Sbpase Derived from Cyanobacteria Exhibits Enhanced Photosynthesis and Mesophyll Conductance to CO2. *PLOS ONE* **10**, e0140928 (2015).
47. Lehmeier, C. *et al.* Cell density and airspace patterning in the leaf can be manipulated to increase leaf photosynthetic capacity. *Plant J.* **92**, 981–994 (2017).
48. Flexas, J. *et al.* Tobacco aquaporin NtAQP1 is involved in mesophyll conductance to CO2in vivo. *Plant J.* **48**, 427–439 (2006).
49. Su, J. & Wu, R. Stress-inducible synthesis of proline in transgenic rice confers faster growth under stress conditions than that with constitutive synthesis. *Plant Sci.* **166**, 941–948 (2004).
50. Zhang, L., McEvoy, D., Le, Y. & Ambrose, C. Live imaging of microtubule organization, cell expansion, and intercellular space formation in Arabidopsis leaf spongy mesophyll cells. *Plant Cell* **33**, 623–641 (2021).
51. Liu, X. *et al.* Global Agricultural Water Scarcity Assessment Incorporating Blue and Green Water Availability Under Future Climate Change. *Earths Future* **10**, e2021EF002567 (2022).
52. Wong, S. C. *et al.* Humidity gradients in the air spaces of leaves. *Nat. Plants* **8**, 971–978 (2022).
53. Long, S. P., Marshall-Colon, A. & Zhu, X.-G. Meeting the Global Food Demand of the Future by Engineering Crop Photosynthesis and Yield Potential. *Cell* **161**, 56–66 (2015).

54. Pathare, V. S. *et al.* Altered cell wall hydroxycinnamate composition impacts leaf- and canopy-level CO2 uptake and water use in rice. *Plant Physiol.* **194**, 190–208 (2024).
55. Pj, F., T, W. D.-A., Zj, B.-H. & Je, G. Increasing water-use efficiency directly through genetic manipulation of stomatal density. *New Phytol.* **207**, (2015).
56. Buckley, C. R., Caine, R. S. & Gray, J. E. Pores for Thought: Can Genetic Manipulation of Stomatal Density Protect Future Rice Yields? *Front. Plant Sci.* **10**, 1783 (2019).
57. Głowacka, K. *et al.* Photosystem II Subunit S overexpression increases the efficiency of water use in a field-grown crop. *Nat. Commun.* **9**, 868 (2018).
58. Lawson, T., Simkin, A. J., Kelly, G. & Granot, D. Mesophyll photosynthesis and guard cell metabolism impacts on stomatal behaviour. *New Phytol.* **203**, 1064–1081 (2014).
59. Patron, N. J. *et al.* Standards for plant synthetic biology: a common syntax for exchange of DNA parts. *New Phytol.* **208**, 13–19 (2015).
60. Pollak, B. *et al.* Loop assembly: a simple and open system for recursive fabrication of DNA circuits. *New Phytol.* **222**, 628–640 (2019).
61. Berardini, T. Z. *et al.* The Arabidopsis information resource: Making and mining the 'gold standard' annotated reference plant genome. *Genes. N. Y. N 2000* **53**, 474–485 (2015).
62. *Agrobacterium Protocols: Volume 2*. vol. 1224 (Springer, New York, NY, 2015).
63. Bustin, S. A. *et al.* The MIQE Guidelines: Minimum Information for Publication of Quantitative Real-Time PCR Experiments. *Clin. Chem.* **55**, 611–622 (2009).
64. Evans, J. R., Caemmerer, S. V., Setchell, B. A. & Hudson, G. S. The Relationship Between CO2 Transfer Conductance and Leaf Anatomy in Transgenic Tobacco With a Reduced Content of Rubisco. *Funct. Plant Biol.* **21**, 475–495 (1994).

65. Amaral, L. I. V. do, Gaspar, M., Costa, P. M. F., Aidar, M. P. M. & Buckeridge, M. S. Novo método enzimático rápido e sensível de extração e dosagem de amido em materiais vegetais. *Hoehnea* **34**, 425–431 (2007).
66. Kondo, M. *et al.* Validation of a phenol-sulfuric acid method in a microplate format for the quantification of soluble sugars in ruminant feeds. *Anim. Sci. J.* **92**, e13530 (2021).
67. Foster, C. E., Martin, T. M. & Pauly, M. Comprehensive compositional analysis of plant cell walls (lignocellulosic biomass) part II: carbohydrates. *J. Vis. Exp. JoVE* 1837 (2010) doi:10.3791/1837.
68. Bethke, G. & Glazebrook, J. Measuring Pectin Properties to Track Cell Wall Alterations During Plant-Pathogen Interactions. *Methods Mol. Biol. Clifton NJ* **1991**, 55–60 (2019).
69. Weyers, J. D. B. & Johansen, L. G. Accurate Estimation of Stomatal Aperture from Silicone Rubber Impressions. *New Phytol.* **101**, 109–115 (1985).
70. Schneider, C. A., Rasband, W. S. & Eliceiri, K. W. NIH Image to ImageJ: 25 years of image analysis. *Nat. Methods* **9**, 671–675 (2012).
71. Tazoe, Y., Von Caemmerer, S., Estavillo, G. M. & Evans, J. R. Using tunable diode laser spectroscopy to measure carbon isotope discrimination and mesophyll conductance to CO2 diffusion dynamically at different CO2 concentrations. *Plant Cell Environ.* **34**, 580–591 (2011).
72. Wang, Y. *et al.* Increased bundle-sheath leakiness of CO2 during photosynthetic induction shows a lack of coordination between the C4 and C3 cycles. *New Phytol.* **236**, 1661–1675 (2022).
73. Lochocki, E. B. PhotoGEA: Photosynthetic Gas Exchange Analysis. **v0.10.0**, (2023).
74. Ubierna, N., Holloway-Phillips, M.-M. & Farquhar, G. D. Using Stable Carbon Isotopes to Study C3 and C4 Photosynthesis: Models and Calculations. in *Photosynthesis: Methods and Protocols* (ed. Covshoff, S.) 155–196 (Springer, New York, NY, 2018). doi:10.1007/978-1-4939-7786-4_10.

855 75. Walker, B., Ariza, L. S., Kaines, S., Badger, M. R. & Cousins, A. B. Temperature response of in vivo
856 Rubisco kinetics and mesophyll conductance in Arabidopsis thaliana: comparisons to Nicotiana
857 tabacum. *Plant Cell Environ.* **36**, 2108–2119 (2013).
858 76. Kromdijk, J. *et al.* Improving photosynthesis and crop productivity by accelerating recovery from
859 photoprotection. *Science* **354**, 857–861 (2016).
860 77. Sharkey, T. D., Bernacchi, C. J., Farquhar, G. D. & Singsaas, E. L. Fitting photosynthetic carbon dioxide
861 response curves for C3 leaves. *Plant Cell Environ.* **30**, 1035–1040 (2007).
862 78. Ellsworth, P. V., Ellsworth, P. Z., Koteyeva, N. K. & Cousins, A. B. Cell wall properties in Oryza sativa
863 influence mesophyll CO2 conductance. *New Phytol.* **219**, 66–76 (2018).
864